Preprint typeset using LaTeX style emulateapj v. 5/2/11

Online-only material : color figures

A NEW BLACK HOLE MASS ESTIMATE FOR OBSCURED ACTIVE GALACTIC NUCLEI

Takeo Minezaki[1] and Kyoko Matsushita[2]

ABSTRACT

We propose a new method for estimating the mass of a supermassive black hole, applicable to obscured Active Galactic Nuclei (AGNs). This method estimates the black hole mass using the width of the narrow core of the neutral FeKα emission line in X-rays and the distance of its emitting region from the black hole based on the isotropic luminosity indicator via the luminosity scaling relation. We collect the line width data of the neutral FeKα line core for seven type-1 AGNs and seven type-2 AGNs obtained by the Chandra High Energy Transmission Grating Spectrometer, which affords the best spectral resolution currently available. Assuming the virial relation between the locations and the velocity widths of the neutral FeKα line core and the broad Hβ emission line, the luminosity scaling relation of the neutral FeKα line core emitting region is estimated. We find that the full width at half maximum of the neutral FeKα line core falls between that of the broad Balmer emission lines and the corresponding value at the dust reverberation radius for most of the type-1 AGNs and for all of the type-2 AGNs. This suggests that significant fraction of photons of the neutral FeKα line core originates between the outer BLR and the inner dust torus in most cases. The black hole mass $M_{\rm BH,FeK\alpha}$ estimated with this method is then compared with other black hole mass estimates, such as the broad emission-line reverberation mass $M_{\rm BH,rev}$ for the type-1 AGNs, the mass $M_{\rm BH,H_2O}$ based on the H_2O maser and the single-epoch mass estimate $M_{\rm BH,pol}$ based on the polarized broad Balmer lines for the type-2 AGNs. We find that $M_{\rm BH,FeK\alpha}$ is consistent with $M_{\rm BH,rev}$ for the most of the type-1 AGNs and with $M_{\rm BH,pol}$ for all of the type-2 AGNs. We also find that $M_{\rm BH,FeK\alpha}$ is correlated well with $M_{\rm BH,H_2O}$ for the type-2 AGNs. These results suggest that $M_{\rm BH,FeK\alpha}$ is a potential indicator of the black hole mass especially for obscured AGNs. In contrast, $M_{\rm BH,FeK\alpha}$ for which the same virial factor as for $M_{\rm BH,rev}$ and $M_{\rm BH,pol}$ is adopted is systematically larger than $M_{\rm BH,H_2O}$ by about a factor of ~ 5, and the possible origins are discussed.

Subject headings: black hole physics — galaxies: nuclei — galaxies: active — galaxies: Seyfert — X-rays: galaxies — polarization

1. INTRODUCTION

The correlation between the mass of the supermassive black holes in the centers of galaxies and the bulge stellar mass or the velocity dispersion (e.g., Kormendy & Richstone 1995; Magorrian et al. 1998; Kormendy & Ho 2013) strongly suggest that the growth of the central supermassive black hole and the evolution of the galaxies are connected. Obscured Active Galactic Nuclei (AGNs) are important targets for studying the AGN-galaxy coevolution because a large number of host galaxies can be investigated in detail being free from the strong central emission from the AGN itself. Moreover, they are of special importance because some types of obscured AGNs such as the ultraluminous infrared galaxies (ULIRGs) have long been anticipated to be in the middle of the evolutionary sequence of AGNs (e.g., Sanders et al. 1988; Sanders & Mirabel 1996; Hopkins et al. 2008). The "new type AGNs" recently found by Ueda et al. (2007), where the central engine is thought to be deeply obscured by a dust torus with an unusually small opening angle, are also interesting for its nature and role in the AGN evolution.

Consequently, measuring the black hole mass in obscured AGNs is important; however, the precise measurement is not straightforward. The position-velocity diagram of the molecular disk surrounding the black hole, obtained by the VLBI observation of the H_2O maser, is considered to be one of the most precise estimate for the black hole mass (e.g., Miyoshi et al. 1995). However, precise alignment between the equatorial plane of the molecular disk and the observer's line of sight is required for the disk H_2O maser to be observable; thus the number of applicable targets is very limited. The single-epoch mass estimate based on the luminosity scaling relation of the broad emission-line region (BLR) (e.g., Laor 1998; McLure & Jarvis 2002; Vestergaard & Peterson 2006) measuring the widths of the polarized broad Balmer emission lines would be widely available for type-2 AGNs. However, a significant fraction of type-2 AGNs does not present the polarized broad Balmer emission lines (Tran 2001). Moreover, this type of measurement might be unavailable for the ULIRGs and the new-type AGNs, whose BLR is largely covered by obscuring materials. A precise estimate of the black hole mass that is widely available for obscured AGNs is desired.

The fluorescent iron Kα line (hereafter, FeKα line) is an almost ubiquitous emission line observable for both obscured and unobscured AGNs (Yaqoob & Padmanabhan 2004; Nandra et al. 2007; Fukazawa et al. 2011). The rest-frame energy of the narrow core of the FeKα emission line is close to that of

[1] Institute of Astronomy, School of Science, University of Tokyo, 2-21-1 Osawa, Mitaka, Tokyo 181-0015, Japan; minezaki@ioa.s.u-tokyo.ac.jp
[2] Department of Physics, Tokyo University of Science, 1-3 Kagurazaka, Shinjuku-ku, Tokyo 162-8601, Japan

neutral or low-ionization-state irons. Considering its narrow line width, the emitting region is supposed to be not very close to the black hole, such as the outer parts of the accretion disk and more distant matter. The large equivalent width indicates both large covering fraction and large optical depth for the emitting region, which suggests that the neutral FeKα line core originates in the dust torus surrounding the central engine in accordance with the unified model of AGNs (e.g., Awaki et al. 1991).

When the width of an emission line and the distance of its emitting region from the black hole are obtained, the black hole mass can be estimated assuming the virial relation. Jiang et al. (2011) assumed that the location of the emitting region of the neutral FeKα line core corresponds to the near-infrared K-band reverberation radius for the inner region of the dust torus, and estimated the black hole mass of 10 type-1 AGNs on the basis of the FeKα line widths and the luminosity scaling relation of the dust reverberation radius to the optical V-band luminosity by Suganuma et al. (2006). They examined the black hole mass on the basis of the neutral FeKα line core by comparing the black hole mass obtained from the broad emission-line reverberation; however, the correlation between them was statistically insignificant, which could be attributable to small sample size and large uncertainties in the FeKα line widths.

Recently, Greene et al. (2010b) and Koshida et al. (2014) presented the luminosity scaling relations of the broad Hβ emission-line reverberation radius and the dust reverberation radius to isotropic luminosity indicators that are unbiased by the obscuration, such as the luminosity of the [O IV] λ25.89 μm emission line $L_{[\mathrm{OIV}]}$, and that of the *Swift* BAT hard X-ray (14–195 keV) band L_{BAT} (e.g., Melèndez et al. 2008; Rigby et al. 2009; Diamond-Stanic et al. 2009). Using these radius-luminosity scaling relations, it becomes possible to derive the radius of the emitting region of the neutral FeKα line core for obscured AGNs.

In this paper, we estimate the black hole mass of both obscured and unobscured AGNs on the basis of the line width of the neutral FeKα line core and the luminosity scaling relation of its emitting region radius with the [O IV] λ25.89 μm emission-line luminosity. Then, the estimated black hole mass was examined by comparing them with other black hole mass estimates that have been established. We assume the cosmology of $H_0 = 73$ km s^{-1} Mpc^{-1}, $\Omega_m = 0.27$, and $\Omega_\Lambda = 0.73$ according to Spergel et al. (2007) throughout this paper.

2. TARGETS

We collect the line width data of the neutral FeKα line core obtained by the *Chandra* High Energy Transmission Grating Spectrometer (HETGS; Markert et al. 1994), which affords the best spectral resolution currently available in the FeKα energy band ($\sim$ 39 eV, or $\sim$ 1860 km s^{-1} in full width at half maximum; FWHM), and we further select target AGNs with other mass estimates of their central supermassive black holes.

For the type-1 AGNs, seven target AGNs whose black hole masses are measured by the reverberation of the broad emission lines are selected out of 12 AGNs, for which the best FWHM constraint for the neutral FeKα line core was obtained by Shu et al. (2010). The type-1 target AGNs and their data are listed in Table 1.

For the type-2 AGNs, four target AGNs whose black hole masses are measured by the VLBI observation of the H_2O maser are selected out of eight AGNs, for which the FWHM of the neutral FeKα line core was measured by Shu et al. (2011). In addition, one type-2 AGN from the 12 AGNs of Shu et al. (2010) and five type-2 AGNs from the eight AGNs of Shu et al. (2011) are also selected, for which the FWHMs of the polarized broad Balmer emission lines are available to obtain the single-epoch black hole mass estimate on the basis of the luminosity scaling relation of the BLR. In total, seven type-2 AGNs are selected because three objects in the $4 + 6$ type-2 AGNs are common. The type-2 target AGNs and their data are listed in Table 2.

3. RESULTS

3.1. *Velocity Width of the Neutral FeKα Line Core*

First, we compare the velocity width of the neutral FeKα line core with that of the broad Balmer emission lines, and that corresponding to the dust reverberation radius to examine the location of its emitting region.

In Figure 1, we plotted the FWHM of the neutral FeKα line core against those of the broad Hβ emission line and the polarized broad Balmer emission lines for the type-1 and type-2 target AGNs, respectively. We also plotted the line that represents the FWHM at the dust reverberation radius observed in the K band, which is estimated by scaling the FWHM of the broad Hβ emission line according to the virial relation based on the systematic difference of the reverberation radii of the broad Hβ emission line and the near-infrared dust emission (Koshida et al. 2014).

As shown in Figure 1, we find that the FWHM of the neutral FeKα line core falls between that of the broad Balmer emission lines and the corresponding value at the dust reverberation radius for all of the type-2 AGNs, and for most of the type-1 AGNs except the only one outlier of NGC 7469. This suggests that significant fraction of photons of the neutral FeKα line core originate between the outer BLR and the inner dust torus in most cases.

3.2. *Luminosity Scaling Relation of the Neutral FeKα Line Core Emitting Region*

As a next step, we scaled the radius-luminosity scaling relation of the broad Hβ emission line according to the systematic difference between the FWHMs of the neutral FeKα line core and the broad Hβ emission line for the type-1 AGNs assuming the virial relation. It is estimated by the linear regression analysis where the slope is fixed to unity, and the best-fit linear regression is $\log \mathrm{FWHM}_{\mathrm{FeK}\alpha} = \log \mathrm{FWHM}_{\mathrm{H}\beta} - 0.186$ ($\pm$0.088) with an additional scatter of 0.11 dex in both directions for the reduced χ^2 to achieve unity. Then, the emitting region radius of the neutral FeKα line core is estimated as

$$\log \mathrm{r}_{\mathrm{FeK}\alpha} = \log \mathrm{r}_{\mathrm{H}\beta} - 0.37\ (\pm 0.18) \qquad (1)$$

according to the virial relation. Koshida et al. (2014) estimated the luminosity scaling relation of the reverberation radii to the luminosity of the [O IV] emission line in the form of $\log r = \alpha + 0.5 \log L_{[\mathrm{OIV}]}/10^{41}$ erg s^{-1}, as $\alpha = -1.94$ ($\pm$0.07) and $\alpha = -1.28$ ($\pm$0.07) for the

reverberation radius of the broad Hβ emission line and the dust reverberation radius observed in the K band, respectively. By scaling the former relation according to Equation (1), the luminosity scaling relation of the emitting region radius of the neutral FeKα line core is estimated as

$$\log r_{\mathrm{FeK}\alpha} = -1.57\ (\pm 0.19) + 0.5 \log L_{[\mathrm{OIV}]}/10^{41}\ \mathrm{erg\ s^{-1}}\ . \quad (2)$$

The radius-luminosity scaling relation for the neutral FeKα line core of Equation (2) is located between the reverberation radii of the broad Hβ emission line and the dust torus emission in the K band as indicated by Figure 1, and we use it for the estimation of the black hole mass in the next section.

3.3. *Estimating the Black Hole Mass from the Neutral FeKα Line Core*

Next, we estimate the black hole mass of both type-1 and type-2 target AGNs using the neutral FeKα line core. The emitting region radius $r_{\mathrm{FeK}\alpha}$ is estimated from $L_{[\mathrm{OIV}]}$ and the radius-luminosity scaling relation of Equation (2) because the hard X-ray flux seems to be attenuated in some heavily obscured AGNs in the targets. The $L_{[\mathrm{OIV}]}$ value is taken from Liu & Wang (2010), on the basis of the original data of Melèndez et al. (2008) and Diamond-Stanic et al. (2009) for most of the targets; however, it is recalculated from the [O IV] emission-line flux of Diamond-Stanic et al. (2009), assuming the redshift-independent distance taken from the NASA/IPAC Extragalactic Database for very nearby objects. In addition, the $L_{[\mathrm{OIV}]}$ of NGC 2110 is calculated from the data of Weaver et al. (2010). We then estimate the black hole mass assuming the virial relation as

$$M_{\mathrm{BH,FeK}\alpha} = f \frac{r_{\mathrm{FeK}\alpha}\sigma^2_{\mathrm{FeK}\alpha}}{G} \quad (3)$$

where f is the virial factor and $\sigma_{\mathrm{FeK}\alpha}$ is the velocity dispersion of the neutral FeKα line core. We adopt $f = 5.5$ following the references of the broad emission-line reverberation for the type-1 target AGNs (Onken et al. 2004; Peterson et al. 2004; Bentz et al. 2006, 2007; Denney et al. 2010; Grier et al. 2012). The velocity dispersion is calculated as $\sigma_{\mathrm{FeK}\alpha} = \mathrm{FWHM}_{\mathrm{FeK}\alpha}/2.35$ because a Gaussian emission-line profile is used for the spectral fitting of the neutral FeKα line core in Shu et al. (2010, 2011). The $L_{[\mathrm{OIV}]}$ and the $M_{\mathrm{BH,FeK}\alpha}$ for the type-1 and type-2 target AGNs are listed in Tables 1 and 2, respectively.

The FWHM of the neutral FeKα line core spreads between that of the broad Hβ line and that corresponding to the dust reverberation radii in most cases. This scatter causes a systematic uncertainty in the $r_{\mathrm{FeK}\alpha}$ derived from the radius-luminosity scaling relation, and also yields ± 0.3 dex or a factor ~ 2 uncertainty in this black hole mass estimates, $M_{\mathrm{BH,FeK}\alpha}$, including the measurement errors of the line widths in the data. As in the case of NGC 7469, in which the FWHM of the neutral FeKα line is significantly larger than that of the broad Hβ line, $M_{\mathrm{BH,FeK}\alpha}$ could be sometimes overestimated.

3.4. *Comparison with Other Black Hole Mass Indicators*

Finally, the black hole mass $M_{\mathrm{BH,FeK}\alpha}$ estimated from the neutral FeKα line core is compared with other estimates of the black hole mass for the same target to examine the consistency between them. For the type-1 AGNs, we compared $M_{\mathrm{BH,FeK}\alpha}$ with the broad emission-line reverberation mass, $M_{\mathrm{BH,rev}}$, and for the type-2 AGNs, we compare it with the mass $M_{\mathrm{BH,H_2O}}$ based on the H_2O maser and the single-epoch mass estimate $M_{\mathrm{BH,pol}}$ based on the polarized broad Balmer lines. The $M_{\mathrm{BH,pol}}$ is calculated in the same way as the $M_{\mathrm{BH,FeK}\alpha}$, except that the radius-luminosity scaling relation of the broad Hβ emission line presented by Koshida et al. (2014) is used. The $M_{\mathrm{BH,rev}}$, $M_{\mathrm{BH,H_2O}}$, $M_{\mathrm{BH,pol}}$, and their references are listed in Tables 1 and 2.

In Figure 2, $M_{\mathrm{BH,FeK}\alpha}$ is plotted against other black hole mass indicators such as $M_{\mathrm{BH,rev}}$, $M_{\mathrm{BH,H_2O}}$, and $M_{\mathrm{BH,pol}}$ for the type-1 and type-2 target AGNs. We then calculated the Pearson's correlation coeffient, and also performed linear regression analysis to $M_{\mathrm{BH,FeK}\alpha}$ and the other black hole mass indicators. The resultant values are listed in Table 3, and the best-fit linear regression lines are also presented in Figure 2.

For the type-1 AGNs, $M_{\mathrm{BH,FeK}\alpha}$ and $M_{\mathrm{BH,rev}}$ are consistent within $\pm 2\sigma$ except for NGC 7469. The best-fit linear regression where the slope is fixed to unity is estimated as

$$\log(M_{\mathrm{BH,FeK}\alpha}/10^{7.5} M_\odot) = -0.15\ (\pm 0.11) + \log(M_{\mathrm{BH,rev}}/10^{7.5} M_\odot)\ , \quad (4)$$

which indicates that the systematic difference between them is within a factor of several tens percent. However, the correlation between $M_{\mathrm{BH,FeK}\alpha}$ and $M_{\mathrm{BH,rev}}$ is not clear as with the preceding study (Jiang et al. 2011). Excluding the clear outlier NGC 7469, the Pearson's correlation coefficient is calculated as $R = 0.701$, which indicates that the confidence level of the correlation is less than 90%. The best-fit linear regression for them is estimated as

$$\log(M_{\mathrm{BH,FeK}\alpha}/10^{7.5} M_\odot) = -0.19\ (\pm 0.17) + 1.52\ (\pm 0.92) \times \log(M_{\mathrm{BH,rev}}/10^{7.5} M_\odot) \quad (5)$$

with an additional scatter in both directions for the reduced χ^2 to achieve unity. The large uncertainty in the slope of the best-fit linear regression also indicates no or a weak correlation between them.

For the type-2 AGNs, $M_{\mathrm{BH,FeK}\alpha}$ are also consistent with $M_{\mathrm{BH,pol}}$ within $\pm 2\sigma$. The best-fit linear regression for $M_{\mathrm{BH,FeK}\alpha}$ and $M_{\mathrm{BH,pol}}$ is estimated as

$$\log(M_{\mathrm{BH,FeK}\alpha}/10^{7.5} M_\odot) = -0.13\ (\pm 0.13) + 1.05\ (\pm 0.25) \times \log(M_{\mathrm{BH,pol}}/10^{7.5} M_\odot) \quad (6)$$

which indicates that the systematic difference between $M_{\mathrm{BH,FeK}\alpha}$ and $M_{\mathrm{BH,pol}}$ is also within a factor of several tens percent. In addition, $M_{\mathrm{BH,FeK}\alpha}$ and $M_{\mathrm{BH,pol}}$ are well correlated and show an approximately proportional relationship, since the slope of the best-fit linear regression is positive more than 3σ uncertainties and close to unity. The Pearson's correlation coefficients are calculated as $R = 0.831$, which indicates that the confidence level of the correlation is more than 95%.

In contrast to the good agreement with $M_{\mathrm{BH,pol}}$, $M_{\mathrm{BH,FeK}\alpha}$ seems to be systematically larger than $M_{\mathrm{BH,H_2O}}$ although they show a clear correlation with the Pearson's correlation coefficient of $R = 0.960$ indicating the confidence level of more than 95%. The best-fit linear regression is estimated as

$$\log(M_{\mathrm{BH,FeK}\alpha}/10^{6.5} M_\odot) = 0.70\ (\pm 0.12) + 1.57\ (\pm 0.33) \times \log(M_{\mathrm{BH,H_2O}}/10^{6.5} M_\odot) \quad (7)$$

which indicates that $M_{\rm BH,FeK\alpha}$ is systematically larger than $M_{\rm BH,H_2O}$ by about a factor of ~ 5. We note that $M_{\rm BH,pol}$ is also larger than $M_{\rm BH,H_2O}$ by a similar factor for the three targets, NGC 1068, NGC 4388, and Circinus, for which both $M_{\rm BH,H_2O}$ and $M_{\rm BH,pol}$ are estimated.

To summarize the results, $M_{\rm BH,FeK\alpha}$ is consistent with $M_{\rm BH,rev}$ for most of the type-1 AGNs and with $M_{\rm BH,pol}$ for all of the type-2 AGNs. $M_{\rm BH,FeK\alpha}$ is correlated well with $M_{\rm BH,pol}$ and $M_{\rm BH,H_2O}$ for the type-2 AGNs, although $M_{\rm BH,H_2O}$ is a systematic smaller than the others. These results suggest that the black hole mass estimate using the neutral FeKα line is a potential indicator of the black hole mass, especially for obscured AGNs.

4. DISCUSSION

4.1. *Systematic Difference of the H_2O maser mass from the Other Black Hole Mass Indicators*

The systematic difference of $M_{\rm BH,H_2O}$ implies an ambiguous issue. Since $M_{\rm BH,H_2O}$ is considered to be the most precise estimate for the black hole mass, then, through the relations of $M_{\rm BH,H_2O}$ with $M_{\rm BH,FeK\alpha}$ and $M_{\rm BH,pol}$, another reliable estimate $M_{\rm BH,rev}$ is suspected to considerably overestimate the black hole mass that is difficult to be accounted for by the uncertainties in the virial factor f (5.5 in this paper and presented by Onken et al. 2004; 5.2 by Woo et al. 2010; 2.8 by Graham et al. 2011; 4.31 by Grier et al. 2013). In this section, the systematic differences between those black hole mass estimates and the possible origins of these differences are discussed.

In fact, the systematic difference between $M_{\rm BH,pol}$ and $M_{\rm BH,H_2O}$ has been indicated by preceding studies. Greene et al. (2010a) measured the stellar velocity dispersion σ_* in the centers of the galaxies hosting type-2 AGNs whose $M_{\rm BH,H_2O}$ was obtained, and found that $M_{\rm BH,H_2O}$ tended to be smaller than the black hole mass that was estimated from σ_* and the $M_{\rm BH}$–σ_* relation of local elliptical galaxies. On the other hand, Zhang et al. (2008) estimated the radius of the BLR from the [O III] luminosity via the luminosity scaling relation of the BLR to estimate $M_{\rm BH,pol}$ of 12 type-2 AGNs, and found that $M_{\rm BH,pol}$ tended to be larger than the black hole mass that was estimated from σ_* via the $M_{\rm BH}$–σ_* relation. According to these results, $M_{\rm BH,pol}$ would be systematically larger than $M_{\rm BH,H_2O}$, as is the case in this study.

Recently, Ho & Kim (2014) presented that the virial factor f of the reverberation-mapped AGN is systematically different between two bulge types of the host galaxies, as $f = 6.3 \pm 1.5$ for classical bulges and ellipticals, and $f = 3.2 \pm 0.7$ for psuedobulges. In fact, the black hole mass of the AGNs with psuedobulges tends to be smaller than that with classical bulges and ellipticals as shown in their Figure 2. Greene et al. (2010a) also argued that the mass of the black hole hosted by later-type and lower-mass galaxies tended to be less massive with larger scatter than that estimated from the $M_{\rm BH}$–σ_* relation for the elliptical galaxies. Since our type-2 AGN targets with the H_2O maser observation tend to have a less massive black hole than the others if $M_{\rm BH,H_2O}$ is correct, then, it is possible that the systematic difference of the target selection partly contributes to the systematic difference between $M_{\rm BH,H_2O}$ and the other black hole mass indicators.

Contrary to these studies, Kuo et al. (2011) estimated the radius of the BLR from the absorption-corrected luminosity in the 2–10 keV X-ray band $L_{2-10\rm keV}$ via the luminosity scaling relation of the BLR to estimate $M_{\rm BH,pol}$ of 4 type-2 AGNs whose $M_{\rm BH,H_2O}$ was obtained by them, and presented that $M_{\rm BH,H_2O}$ and $M_{\rm BH,pol}$ were consistent with each other. In fact, the three targets, NGC 1068, NGC 4388, and Circinus, for which the large systematic difference between $M_{\rm BH,pol}$ and $M_{\rm BH,H_2O}$ is presented in this paper, are included in the targets of Kuo et al. (2011). The reason for the discrepancy between these studies is uncertain, but a difficulty in estimating the luminosity of the central engine $L_{2-10\rm keV}$ for most of the targets with very large X-ray absorbing column density could be suspected, although it was estimated with particular attention.

Assuming both $M_{\rm BH,rev}$ and $M_{\rm BH,H_2O}$ are reliable estimates for the black hole mass, $M_{\rm BH,FeK\alpha}$ and $M_{\rm BH,pol}$ are considered to overestimate the black hole mass in type-2 AGNs. The systematically larger $M_{\rm BH,FeK\alpha}$ for the type-2 AGNs implies that the width of the neutral FeKα line core is systematically larger for the large inclination angle for type-2 AGNs. If the emitting region of the neutral FeKα line core shows an equatorial motion, then the virial factor f in Equation (3) decreases as the inclination angle increases. For example, $f = 2$ at the edge-on view, which is smaller than $f = 5.5$ for type-1 AGNs, is derived assuming an equatorial circular motion. However, it is not so small as to account for the difference of about a factor of ~ 5. Outflow motions toward the equatorial plane might broaden the width of the neutral FeKα line core for type-2 AGNs.

On the other hand, the systematically larger $M_{\rm BH,pol}$ for the type-2 AGNs cannot be attributed to the inclination of AGNs from the point of view of the unified model of AGNs; when the broad emission line is scattered to the observer at the polar region well above the height of the dust torus, the viewing angle of the BLR from the scattering region would be similar to that from the observer for type-1 AGNs. Non-virial motions such as outflows in the scattering region are possible to be contributed, as Young et al. (2007) proposed to explain the broad Hα emission line in the polarized spectrum of the quasar PG 1700+518. However, a common or closely related mechanism to broaden the widths of both of the neutral FeKα line core and the polarized broad Balmer emission lines systematically for type-2 AGNs is required to explain the approximate agreement between $M_{\rm BH,FeK\alpha}$ and $M_{\rm BH,pol}$.

4.2. *Location of the Neutral FeKα Line Core Emitting Region*

As described in Section 3, the FWHM of the neutral FeKα line core falls between the FWHM of the broad Balmer emission lines and the corresponding values at the dust reverberation radius in most cases, which indicates that the emitting region of its major fraction is located between the outer BLR and the inner dust torus. It is suggested by previous studies for some of the target AGNs. For NGC 4151, Takahashi et al. (2002) compared the variation of the continuum and the excess flux around the neutral FeKα line and presented that the emitting region of the excess flux has an extent of 10^{17} cm, or 40 light days, which is consistent with or slightly smaller than the dust reverberation radius (Koshida et al. 2014).

For NGC 5548, Liu et al. (2010) reported that the emitting region of the neutral FeKα line was located between the two reverberation radii of the broad Hβ emission line and the near-infrared dust emission based on its flux variation and line width.

The BLR and the dust torus are considered not to be decoupled from each other but to constitute a continuous structure, and the transition zone of the BLR and the dust torus would be located between the two reverberation radii (Nenkova et al. 2008; Koshida et al. 2009, 2014). In addition, recent reverberation observations of the optical Fe II emission lines presented that its reverberation radius was comparable to or at most twice that of the broad Hβ emission line (Barth et al. 2013; Chelouche et al. 2014), which shows the presence of low ionization iron atoms there.

If the FeKα emitting region constitutes a tight stratified structure with the BLR and the dust torus, a good correlation between the FWHMs of the neutral FeKα line and the broad Balmer emission lines is expected. However, as shown in Figure 1, there appears no clear correlation between them as has been reported by previous studies (Nandra 2006; Shu et al. 2010, 2011). A simple explanation for it would be that the neutral FeKα line is produced in different origins such as the outer accretion disk, the BLR, and the innermost dust torus, and the mixing ratio is different from target to target (e.g., Yaqoob & Padmanabhan 2004; Nandra 2006; Bianchi et al. 2008; Liu et al. 2010; Ponti et al. 2013). On the other hand, Shu et al. (2011) suggested that the neutral FeKα line may originate from a universal region at the same radius with respect to the gravitational radius of the central black hole, because its FWHM is almost constant and independent of the black hole mass. In any case, those uncertainties will result in the possible error of the black hole mass estimated from the neutral FeKα line.

In this study, We used the best spectral resolution data currently available, but the spectral resolution and sensitivity are still limited. As a result, the number of the targets is small and the relatively large uncertainties remain in the FWHM data, which would make it difficult to examine the location of the neutral FeKα line emitting region in more detail. In the near future, the substantial progress is expected by the *ASTRO-H* X-ray satellite (Takahashi et al. 2010), which is capable of unprecedented energy-resolution spectroscopy with superior sensitivity at FeKα band. It will enable us to study more detail on the origin of the neutral FeKα line core by examining the line profile of the neutral FeKα line and its time variation, then it will become able to measure the black hole mass with improved accuracy for a large number of obscured AGNs. The hard X-ray luminosity with precise absorption correction is obviously valuable for the isotropic luminosity indicator because the scaling relations of the reverberation radii to the hard X-ray luminosity are tighter than to the [O IV] luminosity (Koshida et al. 2014).

We thank T. Kawaguchi, M. Yoshida, K. Kawabata, and Y. Fukazawa for useful discussions and comments. We also thank the anonymous referee for valuable comments to improve the manuscript. This research has been partly supported by the Grants-in-Aid of Scientific Research (22540247 and 25287062) of the Ministry of Education, Science, Culture and Sports of Japan, and has made use of the NASA/IPAC Extragalactic Database (NED), which is operated by the Jet Propulsion Laboratory, California Institute of Technology, under contract with the National Aeronautics and Space Administration.

REFERENCES

Awaki, H., Koyama, K., Inoue, H., & Halpern, J. P. 1991, PASJ, 43, 195
Barth, A. J., Pancoast, A., Bennert, V. N., et al. 2013, ApJ, 769, 128
Bentz, M. C., Denney, K. D., Cackett, E. M. et al. 2006, ApJ, 651, 775
Bentz, M. C., Denney, K. D., Cackett, E. M. et al. 2007, ApJ, 662, 205
Bianchi, S., La Franca, F., Matt, G., et al. 2008, MNRAS, 389, L52
Chelouche, D., Rafter, S. E., Cotlier, G. I., Kaspi, S., & Barth, A. J. 2014, ApJ, 783, L34
Denney, K. D., Peterson, B. M., Pogge, R. W., et al. 2010, ApJ, 721, 715
Diamond-Stanic, A. M., Rieke, G. H., & Rigby, J. R. 2009, ApJ, 698, 623
Fukazawa, Y., Hiragi, K., Mizuno, M., et al. 2011, ApJ, 727, 19
Graham, A. W., Onken, C. A., Athanassoula, E., & Combes, F. 2011, MNRAS, 412, 2211
Greene, J. E., Peng, C. Y., Kim, M., et al. 2010, ApJ, 721, 26
Greene, J. E., Hood, C. E., Barth, A. J., Bennert, V. N., Bentz, M. C., Filippenko, A. V., Gates, E., Malkan, M. A., Treu, T., Walsh, J. L., & Woo, J.-H. 2010, ApJ, 723, 409
Greenhill, L. J., Moran, J. M., & Herrnstein, J. R. 1997, ApJ, 481, L23
Greenhill, L. J., Booth, R. S., Ellingsen, S. P., et al. 2003, ApJ, 590, 162
Grier, C. J., Peterson, B. M., Pogge, R. W., et al. 2012, ApJ, 755, 60
Grier, C. J., Martini, P., Watson, L. C., et al. 2013, ApJ, 773, 90
Ho, L. C., & Kim, M. 2014, ApJ, 789, 17
Hopkins, P. F., Hernquist, L., Cox, T. J., & Kereš, D. 2008, ApJS, 175, 356
Jiang, P., Wang, J., & Shu, X. 2011, Science China Physics, Mechanics, and Astronomy, 54, 1354
Kormendy, J., & Richstone, D. 1995, ARA&A, 33, 581
Kormendy, J., & Ho, L. C. 2013, ARA&A, 51, 511
Koshida, S., Yoshii, Y., Kobayashi, Y., et al. 2009, ApJ, 700, L109
Koshida, S., Minezaki, T., et al. 2014, ApJ, 788, 159
Kuo, C. Y., Braatz, J. A., Condon, J. J., et al. 2011, ApJ, 727, 20
Laor, A. 1998, ApJ, 505, L83
Liu, Y., Elvis, M., McHardy, I. M., et al. 2010, ApJ, 710, 1228
Liu, T., & Wang, J.-X. 2010, ApJ, 725, 2381
Lodato, G., & Bertin, G. 2003, A&A, 398, 517
Magorrian, J., Tremaine, S., Richstone, D., et al. 1998, AJ, 115, 2285
Markert, T. H., Canizares, C. R., Dewey, D., et al. 1994, Proc. SPIE, 2280, 168
McLure, R. J., & Jarvis, M. J. 2002, MNRAS, 337, 109
Melèndez, M., Kraemer, S. B., Armentrout, B. K., Deo, R. P., Crenshaw, D. M., Schmitt, H. R., Mushotzky, R. F., Tueller, J., Markwardt, C. B. & Winter, L. 2008, ApJ, 682, 94
Miyoshi, M., Moran, J., Herrnstein, J., et al. 1995, Nature, 373, 127
Moran, E. C., Barth, A. J., Kay, L. E., & Filippenko, A. V. 2000, ApJ, 540, L73
Moran, E. C., Barth, A. J., Eracleous, M., & Kay, L. E. 2007, ApJ, 668, L31
Nandra, K. 2006, MNRAS, 368, L62

Nandra, K., O'Neill, P. M., George, I. M., & Reeves, J. N. 2007, MNRAS, 382, 194
Nenkova, M., Sirocky, M. M., Nikutta, R., Ivezić, Ž., & Elitzur, M. 2008, ApJ, 685, 160
Nishiura, S., & Taniguchi, Y. 1998, ApJ, 499, 134
Oliva, E., Marconi, A., Cimatti, A., & Alighieri, S. D. S. 1998, A&A, 329, L21
Onken, C. A., Ferrarese, L., Merritt, D., et al. 2004, ApJ, 615, 645
Peterson, B. M., Ferrarese, L., Gilbert, K. M., et al. 2004, ApJ, 613, 682
Ponti, G., Cappi, M., Costantini, E., et al. 2013, A&A, 549, A72
Rigby, J. R., Diamond-Stanic, A. M., & Aniano, G. 2009, ApJ, 700, 1878
Sanders, D. B., Soifer, B. T., Elias, J. H., et al. 1988, ApJ, 325, 74
Sanders, D. B., & Mirabel, I. F. 1996, ARA&A, 34, 749
Shen, Y., & Ho, L. C. 2014, Nature, 513, 210
Shu, X. W., Yaqoob, T., & Wang, J. X. 2010, ApJS, 187, 581
Shu, X. W., Yaqoob, T., & Wang, J. X. 2011, ApJ, 738, 147
Spergel, D. N., Bean, R., Doré, O., et al. 2007, ApJS, 170, 377
Suganuma, M., Yoshii, Y., Kobayashi, Y., et al. 2006, ApJ, 639, 46
Takahashi, K., Inoue, H., & Dotani, T. 2002, PASJ, 54, 373
Takahashi, T., Mitsuda, K., Kelley, R., et al. 2010, Proc. SPIE, 7732,
Tran, H. D. 1995, ApJ, 440, 565
Tran, H. D. 2001, ApJ, 554, L19
Ueda, Y., Eguchi, S., Terashima, Y., et al. 2007, ApJ, 664, L79
Vestergaard, M., & Peterson, B. M. 2006, ApJ, 641, 689
Weaver, K. A., Meléndez, M., Mushotzky, R. F., et al. 2010, ApJ, 716, 1151
Woo, J.-H., Treu, T., Barth, A. J., et al. 2010, ApJ, 716, 269
Yaqoob, T., & Padmanabhan, U. 2004, ApJ, 604, 63
Young, S., Hough, J. H., Efstathiou, A., et al. 1996, MNRAS, 281, 1206
Young, S., Axon, D. J., Robinson, A., Hough, J. H., & Smith, J. E. 2007, Nature, 450, 74
Zhang, S.-Y., Bian, W.-H., & Huang, K.-L. 2008, A&A, 488, 113

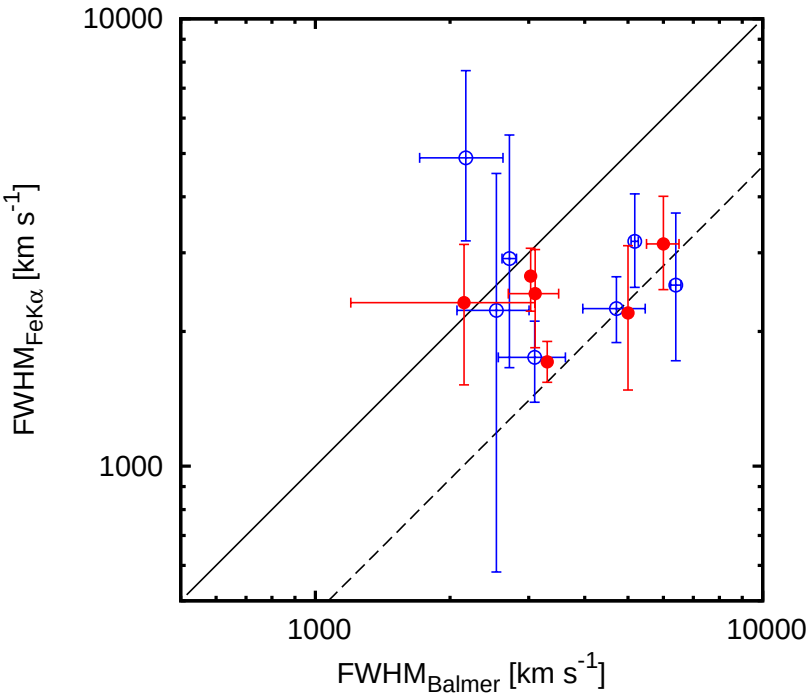

FIG. 1.— The FWHM of the neutral FeKα line core against that of the broad Balmer emission lines. The open circles (colored blue in the online version) represent the broad Hβ emission line for the type-1 AGNs, and the filled circles (colored red in the online version) represent the polarized broad Balmer emission lines for the type-2 AGNs. The solid line represents unity, and the dashed line represents the FWHM at the K-band dust reverberation radius (Koshida et al. 2014). (A color version of this figure is available in the online journal.)

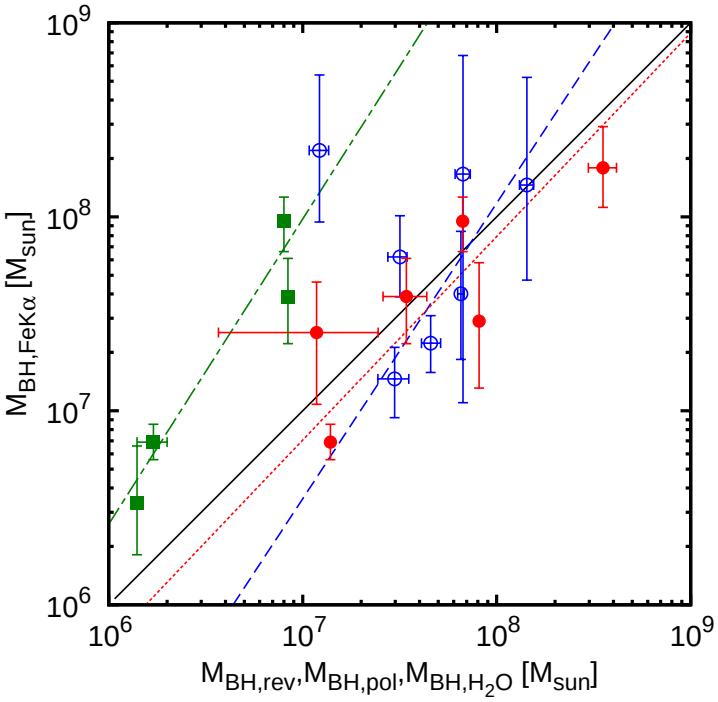

FIG. 2.— The black hole mass estimate based on the neutral FeKα line core, $M_{\rm BH,FeK\alpha}$, and other black hole mass estimates. The open circles (colored blue in the online version) represent the broad emission-line reverberation mass, $M_{\rm BH,rev}$ for the type-1 AGNs. The filled boxes (colored green in the online verseion) represent the black hole mass based on the VLBI observation of the H_2O maser, $M_{\rm BH,H_2O}$, and the filled circles (colored red in the online version) represent the single-epoch mass estimate based on the polarized broad Balmer emission lines, $M_{\rm BH,pol}$, for the type-2 AGNs. The solid line represents unity, and the dashed , dot-dashed, and dotted lines (colored blue, green, and red, respectively, in the online version) represent the best-fit linear regression lines of $M_{\rm BH,FeK\alpha}$ to $M_{\rm BH,rev}$, $M_{\rm BH,H_2O}$, and $M_{\rm BH,pol}$, respectively. (A color version of this figure is available in the online journal.)

TABLE 1
List of the target type-1 AGNs

Object	$\mathrm{FWHM_{FeK\alpha}}$ km s^{-1}	log $L_{[\mathrm{OIV}]}$ erg s^{-1}	$M_{\mathrm{BH,FeK\alpha}}$ $10^7 M_\odot$	$\mathrm{FWHM_{H\beta}}$ km s^{-1}	$M_{\mathrm{BH,rev}}$ $10^7 M_\odot$	refs[a]
3C 120	2230^{+2280}_{-1650}	42.42	17^{+51}_{-16}	2539 ± 466	$6.70^{+0.60}_{-0.60}$	1
NGC 3516	3180^{+880}_{-670}	40.95	$6.2^{+3.9}_{-2.3}$	5175 ± 96	$3.17^{+0.28}_{-0.42}$	2
NGC 3783	1750^{+360}_{-360}	40.73	$1.46^{+0.66}_{-0.54}$	3093 ± 529	$2.98^{+0.54}_{-0.54}$	3
NGC 4151	2250^{+400}_{-360}	40.66	$2.23^{+0.86}_{-0.66}$	4711 ± 750	$4.57^{+0.57}_{-0.47}$	4
NGC 5548	2540^{+1140}_{-820}	40.96	$4.0^{+4.4}_{-2.2}$	6396 ± 167	$6.54^{+0.26}_{-0.25}$	5
Mrk 509	2910^{+2590}_{-1250}	41.85	15^{+38}_{-10}	2715 ± 101	$14.3^{+1.2}_{-1.2}$	3
NGC 7469	4890^{+2770}_{-1700}	41.30	22^{+32}_{-13}	2169 ± 459	$1.22^{+0.14}_{-0.14}$	3

References. — (1) Grier et al. (2012); (2) Denney et al. (2010); (3) Peterson et al. (2004); (4) Bentz et al. (2006); (5) Bentz et al. (2007).

[a] References for FWHM of the broad Hβ emission line, $\mathrm{FWHM_{H\beta}}$, and the black hole mass from the broad emission-line reverberation, $M_{\mathrm{BH,rev}}$.

TABLE 2
List of the target type-2 AGNs

Object	$\mathrm{FWHM_{FeK\alpha}}$ km s^{-1}	log $L_{[\mathrm{OIV}]}$[a] erg s^{-1}	$M_{\mathrm{BH,FeK\alpha}}$ $10^7 M_\odot$	$\mathrm{FWHM_{pol}}$ km s^{-1}	refs[b]	$M_{\mathrm{BH,pol}}$ $10^7 M_\odot$	$M_{\mathrm{BH,H_2O}}$ $10^7 M_\odot$	refs[c]
NGC 1068	2660^{+410}_{-440}	41.67	$9.5^{+3.2}_{-2.9}$	3030	1	6.7	$0.80^{+0.03}_{-0.03}$	8
NGC 2110	2320^{+810}_{-800}	40.76	$2.5^{+2.1}_{-1.5}$	2150 ± 950[d]	2	$1.2^{+1.3}_{-0.8}$	...	...
Mrk 3	3140^{+870}_{-660}	41.93	18^{+11}_{-7}	6000 ± 500	3	35^{+6}_{-6}	...	...
NGC 4388	2430^{+620}_{-590}	41.05	$3.9^{+2.2}_{-1.7}$	3100 ± 400	4	$3.4^{+0.9}_{-0.8}$	$0.84^{+0.02}_{-0.02}$	9
NGC 4507	2200^{+910}_{-720}	40.97	$2.9^{+2.9}_{-1.6}$	5000	5, 6	8.1	...	...
NGC 4945	2780^{+1110}_{-740}	38.69	$0.34^{+0.32}_{-0.16}$	...	...	...	0.14	10
Circinus ·	1710^{+190}_{-170}	40.16	$0.69^{+0.16}_{-0.13}$	3300	7	1.4	$0.17^{+0.03}_{-0.03}$	11

References. — (1)Nishiura & Taniguchi (1998); (2)Moran et al. (2007); (3) Tran (1995); (4) Young et al. (1996); (5) Moran et al. (2000); (6) Shu et al. (2011); (7) Oliva et al. (1998); (8) Lodato & Bertin (2003); (9) Kuo et al. (2011); (10) Greenhill et al. (1997); (11) Greenhill et al. (2003).

[a] The same distance as that of the $M_{\mathrm{BH,H_2O}}$ reference is adopted when available.

[b] References for FWHM of the polarized broad Balmer emission lines, $\mathrm{FWHM_{pol}}$.

[c] References for the black hole mass based on the H_2O maser observation, $M_{\mathrm{BH,H_2O}}$.

[d] The average FWHM of the polarized Hβ emission line and the core component of the polarized Hα emission line.

TABLE 3
Correlation coefficients and linear regressions to $M_{\mathrm{BH,FeK\alpha}}$

$M_{\mathrm{BH,ref}}$	n[a]	R[b]	log $M_{\mathrm{BH},0}$ [$M_\odot$] [c]	a[c]	b[c]
$M_{\mathrm{BH,rev}}$[d]	6	0.701	7.5	-0.19 ± 0.17	1.52 ± 0.92
				-0.15 ± 0.11	1.0 (fixed)
$M_{\mathrm{BH,pol}}$	6	0.831	7.5	-0.13 ± 0.13	1.05 ± 0.25
				-0.12 ± 0.11	1.0 (fixed)
$M_{\mathrm{BH,H_2O}}$	4	0.960	6.5	0.70 ± 0.12	1.57 ± 0.33
				0.73 ± 0.14	1.0 (fixed)

[a] The number of the data.

[b] The Pearson's correlation coefficient.

[c] The fitted model is $\log(M_{\mathrm{BH,FeK\alpha}}/M_{\mathrm{BH},0}) = a + b \times \log(M_{\mathrm{BH,ref}}/M_{\mathrm{BH},0})$, where a and b are the parameters to be fitted.

[d] NGC 7469 was excluded from the calculations of the correlation coefficient and the linear regression.